Astronomy & Astrophysics

XMM-*Newton* unveils the complex iron Kα region of Mrk 279

E. Costantini[1], J. S. Kaastra[1,2], K. Korista[3], J. Ebrero[1], N. Arav[4], G. Kriss[5], and K. C. Steenbrugge[6]

[1] SRON National Institute for Space Research, Sorbonnelaan 2, 3584 CA Utrecht, The Netherlands
   e-mail: e.costantini@sron.nl
[2] Astronomical Institute, Utrecht University, PO Box 80000, 3508 TA Utrecht, The Netherlands
[3] Department of Physics, Western Michigan University, Kalamazoo, MI 49008, USA
[4] Department of Physics, Virginia Tech, Blacksburg, VA 24061, USA
[5] Space Telescope Science Institute, 3700 San Martin Drive, Baltimore, MD 21218, USA
[6] University of Oxford, St John's College Research Centre, Oxford, OX1 3JP, UK

ABSTRACT

We present the results of a ~160 ks-long XMM-*Newton* observation of the Seyfert 1 galaxy Mrk 279. The spectrum shows evidence of both broad and narrow emission features. The Fe Kα line may be equally well explained by a single broad Gaussian (*FWHM* ~ 10 000 km s^{-1}) or by two components: an unresolved core plus a very broad profile (*FWHM* ~ 14 000 km s^{-1}). For the first time we quantified, via the "locally optimally emitting cloud" model, the contribution of the broad line region (BLR) to the absolute luminosity of the broad component of the Fe Kα at 6.4 keV. We find that the contribution of the BLR is only ~3%. In the two-line component scenario, we also evaluated the contribution of the highly ionized gas component, which produces the Fe XXVI line in the iron K region. This contribution to the narrow core of the Fe Kα line is marginal <0.1%. Most of the luminosity of the unresolved, component of Fe Kα may come from the obscuring torus, while the very-broad associated component may come from the accretion disk. However, models of reflection by cold gas are difficult to test because of the limited energy band. The Fe XXVI line at 6.9 keV is consistent to be produced in a high column density ($N_{\rm H}$ ~ 10^{23} cm^{-2}), extremely ionized (log ξ ~ 5.5−7) gas. This gas may be a highly ionized outer layer of the torus.

Key words. galaxies: individual: Mrk 279 – galaxies: Seyfert – quasars: absorption lines – quasars: emission lines – X-rays: galaxies

1. Introduction

The X-ray spectrum of active galactic nuclei (AGN) bears the signature of different environments in the vicinity of the supermassive black hole. In particular, the emission features detected in an X-ray spectrum are believed to arise in different environments, with dramatically distinct physical characteristics of temperature and density. Narrow emission line profiles (especially from C, N, O He-like and H-like ions), not significantly variable on a short time-scale, may form in the far narrow-line region (e.g. Pounds et al. 2004). The broad symmetric line profiles, the more and more often detected in AGN spectra (Kaastra et al. 2002; Ogle et al. 2004; Steenbrugge et al. 2005; Costantini et al. 2007, hereinafter C07), are consistent to be produced, at least in one case, within the broad line region (C07), which is ≈$5.6L_{42}^{1/2}$ light days away from the central black hole (*L* is the luminosity of C IV in units of 10^{42} erg s^{-1}, Peterson 1993). Emission from the accretion disk, located in the proximity of the black hole, has been extensively studied via the iron Kα line at 6.4 keV. For this line, relativistic effects result in a skewed and asymmetric line profile (e.g. Tanaka et al. 1995; Young et al. 2005; Wilms et al. 2001). Recently, relativistic profiles have been reported also for other lines, in particular O VIII (Branduardi-Raymont et al. 2001; Kaastra et al. 2002; Ogle et al. 2004; Steenbrugge et al. 2009). However, a contribution to the line emission from other AGN regions (NLR, BLR and molecular torus) add up to these relativistic profiles. A narrow and not variable component, probably originating far from the black hole, has been disentangled from the Fe Kα line (Yaqoob & Padmanabhan 2004;

Jiménez-Bailón et al. 2005). This component is predicted in the unification model (Antonucci & Miller 1985) as produced in a high-column density, cold region, about 1 pc away from the black hole (e.g. Krolik & Kallman 1987; Krolik et al. 1994) and then scattered into our line of sight (e.g. Ghisellini et al. 1994). An unresolved Fe Kα line and the associated reflection seems indeed to be ubiquitous in bright type 1 objects (Nandra et al. 2007).

As the *FWHM* of the narrow core is compatible with the width of the UV/optical broad lines (Yaqoob & Padmanabhan 2004), a contribution to the broad component from the BLR is in principle possible. However, considering individual sources, no evident correlation between the *FWHM* of neither the hydrogen Hα or Hβ, supposed to be entirely formed in the BLR, has been found (Sulentic et al. 1998; Nandra 2006). These results are based on optical and X-ray data not simultaneously collected. In NGC 7213, using simultaneous observations, the Hα and the resolved iron line shared the same value of the *FWHM* (Bianchi et al. 2008).

Mrk 279 is a bright Seyfert 1 galaxy (*F* ~ 2.55 × 10^{-11} erg cm^{-2} s^{-1}, this study), extensively studied in X-rays (C07 and references therein). C07, using *Chandra*-LETGS data of this source, for the first time quantified the contribution of the BLR to the soft X-ray spectrum. Indeed, thanks to the simultaneous observation of the broad lines in the UV band by HST-STIS and FUSE (Gabel et al. 2005) the ionization structure of the BLR has been determined using the "locally optimally emitting clouds" model (LOC, Baldwin et al. 1995). This allowed to infer the X-ray broad lines luminosities, that were then

Table 1. XMM-*Newton* observation log.

Orbit	Exp (ks)	Exp net (ks)	Date dd-mm-yy	Epic-PN rate c/s (0.3–10 keV)
1087	59.3	27.4	15 − 11 − 05	25.7
1088	59.7	32.0	17 − 11 − 05	21.6
1089	38.0	15.5	19 − 11 − 05	23.5

Notes. The orbit number, the nominal exposure, the net exposure, the date and the 2–10 keV Epic-PN background-subtracted count rates are listed.

contrasted with the LETGS data. C07 found that the broad lines observed in the soft X-ray spectrum (where the O VII triplet was the most prominent one) were consistent to be entirely formed in the BLR. The average peak of production of the X-ray lines is possibly ∼10 times closer in with respect to the UV lines, implying a larger Keplerian width for the X-ray lines. Unfortunately, the limited LETGS energy band prevented C07 to study the iron Kα region. Here we present a detailed study of the X-ray spectrum of Mrk 279 as observed by XMM-*Newton*, focusing mainly on the emission components and the 6.4–7 keV region.

The paper is organized as follows. Section 2 is devoted to the spectral analysis of the data. In Sect. 3 we model the emission spectrum evaluating, for each component, the contribution to the Fe Kα line. In Sect. 4 we discuss our results and in Sect. 5 we present the conclusions. The cosmological parameters used are: $H_0 = 70$ km s^{-1} Mpc^{-1}, $\Omega_m = 0.3$, and $\Omega_\Lambda = 0.7$. The abundances were set to solar following Anders & Grevesse (1989) prescriptions. The redshift is 0.0305 (Scott et al. 2004). The quoted errors are 68% confidence errors ($\Delta\chi^2 = 1$), unless otherwise stated.

2. The data analysis

The observation of Mrk 279 was spread over 3 orbits on November 15–19, 2005. In Table 1 we report the observation log. The data were processed with the standard SAS pipeline (SAS 7.0) and filtered for any background flares. The Epic-PN exposure time in small-window mode reduced the exposure time from the original 160 ks to 110 ks. After the background filtering we obtained a net exposure time of ∼75 ks. The light curve of the three time intervals is displayed in Fig. 1 in the soft (0.3–2 keV) and hard (2–10 keV) band. The maximal variation is about 36% in both energy bands. To increase the statistics, we combined the Epic-PN data after verifying that the physical parameters of the modeling were the same for the three separate data sets. Epic-MOS1 camera was set in timing mode. Due to still existing energy gain uncertainties in this mode, we did not analyze these data further. Epic-MOS2 were collected in imaging mode that resulted in about 61 ks of net observation, after filtering out short high background episodes. For both Epic-PN and MOS2 we imposed at least 20 counts per channel to allow the use of the χ^2 minimization.

The RGS total useful exposure time is about 110 ks. Each RGS data set has been rebinned by a factor 5 which resulted in a bin size of ∼0.07 Å and signal-to-noise ratio of 10 for each set of data that were simultaneously fitted. The spectral analysis was carried out using the fitting package SPEX[1] (ver 2.0).

---

[1] http://www.sron.nl/divisions/hea/spex/version2.0/release/
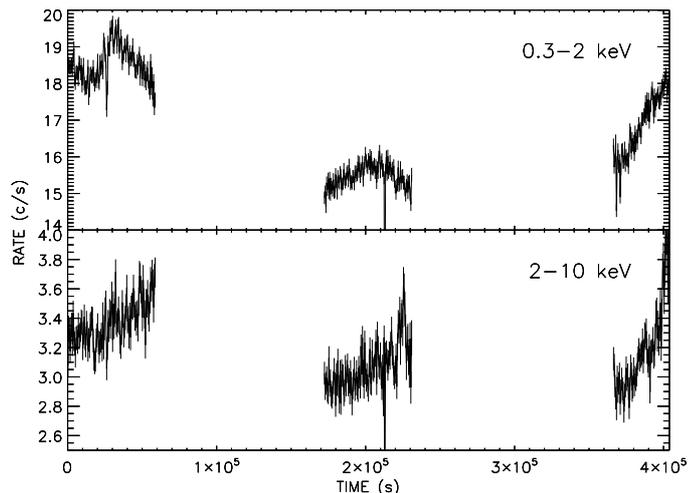
Fig. 1. Epic-PN light curves in the 0.3–2 and 2–10 keV band. The maximal variation is about 36%.

Table 2. Best-fit continuum parameters for a phenomenological model.

		PN	MOS2
T_{mbb}	keV	0.16 ± 0.02	0.12 ± 0.02
Γ_1		2.08 ± 0.01	2.03 ± 0.02
Γ_2		1.75 ± 0.01	1.82 ± 0.03
E_0	keV	2.31 ± 0.04	2.0 ± 0.1
χ^2/ν		281/234	262/208

Notes. Epic-PN and MOS2 fitted separately. The reduced χ^2 refer here to the final best fit.

In the following we describe first the underlying continuum, then the emission line spectrum and finally the absorption features which furrow the spectrum.

2.1. The continuum

The continuum has been first determined using Epic-PN. A single powerlaw fit, modified by Galactic absorption is unacceptable ($\chi^2/\nu > 34$, where ν is the number of degrees of freedom). This fit produces systematic residuals both at soft and hard energies, in addition to narrow features both in absorption and emission. We then added a black body component, modified by coherent Compton scattering (Kaastra & Barr 1989). The reduced χ^2 is again unacceptable ($\chi^2/\nu \sim 6$). The residuals show that a broad band component is still missing. We then substituted the simple powerlaw model with a broken power law, obtaining an acceptable description of the continuum. The reduced χ^2, considering only the best-fit continuum, without narrow emission/absorption features, is $\chi^2/\nu \sim 2.5$. The parameters of this phenomenological interpretation of the continuum are listed in Table 2 and the fit shown in Fig. 2. The parameters in Table 2 and reduced χ^2 refer to the total best fit, including emission and absorption features, as described below (Sects. 2.2, 2.3).

For comparison, we analyzed also MOS2 data, with the caveat that deviation from the Epic-PN best fit may occur, especially at the low ($E < 0.5$ keV) and high energy ($E > 8$ keV) ends of the band, and at the instrumental gold edge around 2 keV[2]. The final MOS2 best-fit parameters are shown in Table 2. The parameters agree well with the Epic-PN fit, albeit with some

---

[2] Several examples are provided at http://xmm2.esac.esa.int/cgi-bin/ept/preview.pl
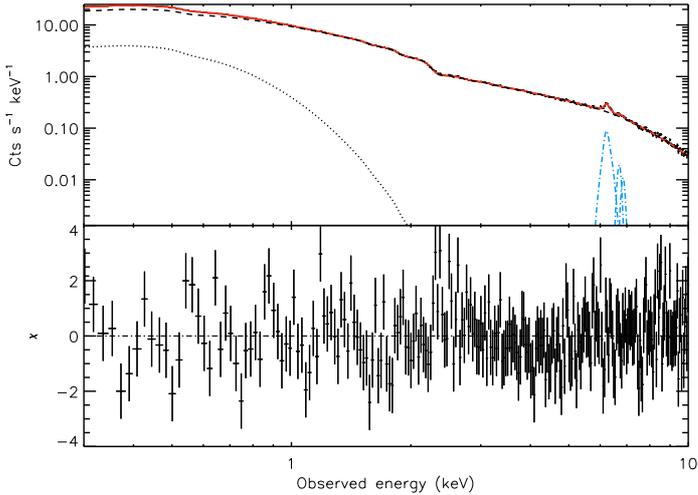
Fig. 2. Best fit for the Epic-PN data. The model includes a modified black body (dotted line), a broken powerlaw (dashed line), both absorbed by ionized gas, a broad Fe Kα (see Sect. 2.2) line and two narrow lines at 6.9 and 7.05 keV (dash-dotted lines).

differences, which we ascribe to the cross calibration mismatch between the MOS and PN cameras.

2.2. The emission line spectrum

We see evidence of a range of broad and narrow emission lines both in the RGS and in the Epic spectra. Here we refer as narrow lines the ones which are unresolved by Epic-PN (i.e. $FWHM < 7000 \, \mathrm{km \, s^{-1}}$), but may be resolved by RGS. Then the broad lines ($FWHM > 7000 \, \mathrm{km \, s^{-1}}$) are instead resolved also by Epic. Finally, the very broad lines are the ones with $FWHM \sim 14\,000 \, \mathrm{km \, s^{-1}}$. The only example of the latter in the present data is the broad, possibly relativistically smeared, component of the iron line at 6.4 keV.

In our previous study broad emission from a blend of the O VII triplet lines was very significantly detected (at $\sim 6\sigma$, C07). We therefore looked for such evidence in the present RGS data. We fix the wavelength of the line centroid ($\lambda = 21.9$ Å) to the values found in C07. We also fix the *FWHM* of the broad feature, which could not be resolved in the individual O VII lines, to the previously measured value: 1.4 Å, corresponding to about $19\,000 \, \mathrm{km \, s^{-1}}$ for the blend. We find that the intrinsic line luminosity decreased with respect to the 2003 observation going from 50 ± 8 to 13 ± 7 in units of $10^{40} \, \mathrm{erg \, s^{-1}}$. The same line luminosity is measured also using the three RGS data sets separately. The inclusion of the line improves the fit by $\Delta\chi^2/\Delta\nu \sim 6/1$, corresponding to only 2.4σ significance. The broad line is also a necessary emission component to correctly fit some underlying absorption features (e.g. O V, O VI and O VII), important in the global fitting of the ionized absorber parameters (Fig. 3). The inclusion of this low-ionization absorber alone improves the fit of the RGS spectrum by $\Delta\chi^2/\Delta\nu \sim 58/3$.

In the RGS band we detect the narrow O VII forbidden line with a flux ($9 \pm 6 \times 10^{-15} \, \mathrm{erg \, cm^{-2} \, s^{-1}}$), consistent with the *Chandra* measurement (C07). The line is marginally detected (Table 3), probably because of a neighboring bad pixel. For other relevant narrow lines, such as O VIII Lyα, Ne IX and Ne X, we only obtain upper limits on the luminosity (Table 3).

Both the PN and MOS2 spectra show a complex structure between 6.4 and 7 keV: a prominent Fe K α line at ~ 6.4 keV (rest-frame) and a broad emission feature, consistent with a blend of Fe XXVI and Fe Kβ at 6.90 ± 0.06 keV and 7.05 ± 0.05 keV

Table 3. List of line luminosities as measured by Epic-PN (inst. 1) and RGS (inst. 2).

Ion	Rest wavelength (Å)	Lum$_{obs}$ (10^{40} erg s^1)	F-test %	Inst.
narrow lines				
Fe Kβ	1.75	6.6 ± 2.8	89.0	1
Fe XXVI Lyα	1.77	10.0 ± 2.7	99.98	1
Fe XXV f.	1.85	<4.7	. . .	1
Fe Kα[1]	1.93	12.0 ± 7.0	>99.99	1
Ne X	12.14	<1.2	. . .	2
Ne IX f.	13.69	<1.25	. . .	2
O VIII Lyα	18.97	<1.0	. . .	2
O VII f.	22.10	3.1 ± 2.0	89.0	2
N VII Lyα	24.78	<3.1	. . .	2
N VI f.	29.53	<1.18	. . .	2
broad lines				
O VII triplet[2]	21.9	13 ± 7	95.0	2
Fe Kα[3]	1.93 ± 0.03	61 ± 6	>99.99	1

Notes. We list the ion, the rest-frame wavelength, the intrinsic luminosity and their significance, for narrow and broad lines. [1] Only narrow, unresolved component in a two-lines model . [2] Blend of the O VII triplet lines .[3] Single Gaussian with free line-width model.
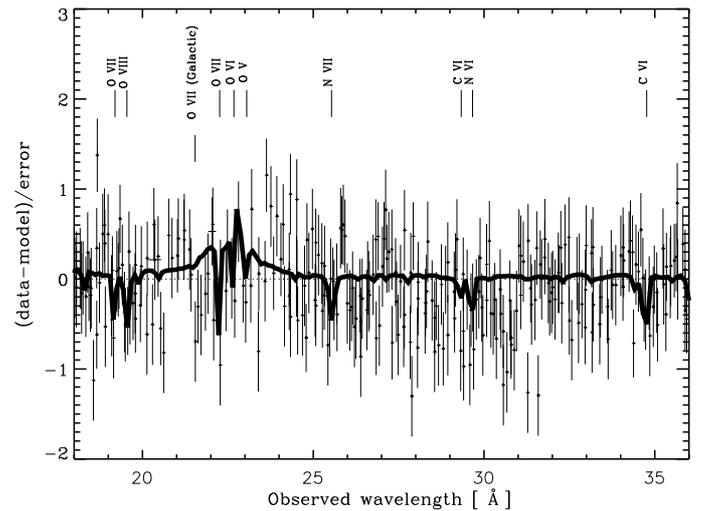
Fig. 3. RGS spectrum in the O VII region in terms of ratio from a continuum fit. For display purpose, only the rebinned data from orbit 1087 and 1088 are shown. The measurements reported in the paper are based on the full RGS exposure. The labels indicate some of the main features of the warm absorber.

respectively (Fig. 4, upper panel). Because the MOS2 spectral analysis deliver a slightly different powerlaw slope at energies >2 keV (Table 2), and the data are affected by lower statistics, we restrict the iron line analysis to the Epic-PN data only. At first we modeled the Fe Kα line with a single unresolved Gaussian. Although the general fit improves ($\chi^2/\nu = 371/243 \sim 1.5$), this model does not provide a good fit for the line, as evident in Fig. 4 (lower panel). Next, we considered the line as composed of an unresolved Gaussian and a very broad component, leading to a significant improvement of the fit ($\Delta\chi^2/\Delta\nu = 32/3$, Table 4). The very broad component has a *FWHM* of 0.29 ± 0.04 keV, corresponding to $\sim 14\,000 \, \mathrm{km \, s^{-1}}$. We tested this very broad component of the Fe Kα line against a relativistically smeared profile (Laor 1991). With this model, the line should be viewed at an angle of $\sim 15°$, with a radial emissivity law r^{-q}, with $q \sim 1.5$
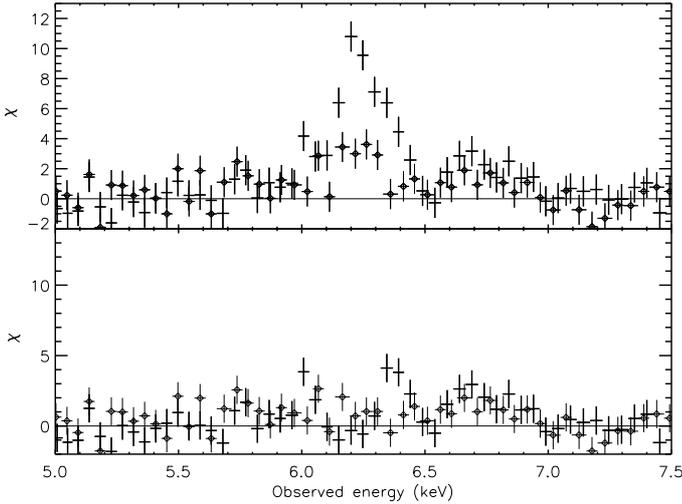
Fig. 4. *Upper panel*: residuals, in terms of σ to the continuum in the iron line region as observed by Epic-PN. Three features are evident: a prominent Fe Kα line and weaker lines identified as Fe XXVI and Fe Kβ. *Lower panel*: residuals, in terms of σ after the inclusion of a narrow line at 6.4 keV. The Epic-PN data are identified by simple crosses, and the MOS2 data by diamonds.

Table 4. Parameters for the very broad component of the Fe Kα line in a two-components model.

		Gauss[1]	Laor[2]
E	keV	6.41 ± 0.01	6.47 ± 0.03
$FWHM$	eV	0.29 ± 0.04	...
Lum	10^{41} erg s^{-1}	4.64 ± 0.16	5.0 ± 0.7
q		...	1.5 ± 0.5
i	deg	...	15 ± 7
χ^2/ν		339/240	334/239

Notes. Third column: one Gaussian with free width. Fourth column: profile including relativistic effects. The reduced χ^2 refers to an intermediate fit (see Sect. 2.2). [1] We list the energy of the centroid, the luminosity of the line and the $FWHM$. [2] We list the energy of the centroid, the luminosity of the line, the emissivity law, q and the inclination angle, i.

(Fig. 5, Table 4). These parameters mimic a regular, almost symmetric, line profile (e.g. Reynolds & Nowak 2003). The statistical improvement with respect to a simple very-broad Gaussian is: $\Delta\chi^2/\Delta\nu \sim 5/1$, corresponding to $\sim 2.2\sigma$. For the Fe Kα feature, we considered also a single Gaussian with the width free to vary (Table 3). The line centroid is 6.41 ± 0.08 in the rest frame of the source, and the intrinsic luminosity is $61 \pm 6 \times 10^{40}$ erg s^{-1}. The line is resolved by Epic-PN, with a $FWHM$ of 0.21 ± 0.03 keV (corresponding to $\sim 10\,000 \pm 1000$ km s^{-1}). The statistical improvement with respect to a single unresolved line is $\Delta\chi^2/\Delta\nu = 37/1$.

The inclusion of other two narrow lines, at the energy of the Fe XXVI and the Fe Kβ further improves the fit by $\Delta\chi^2/\Delta\nu = 31/2$. For consistency, we tested the Laor model, with the same line parameters, to the Fe Kβ, fixing the line ratio to 0.135 (Yaqoob et al. 2007; Palmeri et al. 2003). As expected the flux of a broad Fe Kβ line has a negligible effect on the fit, therefore we ignore this additional component in subsequent fits. This negligible contribution of a broad profile of the Fe Kβ also strengthens our assumption that the bump seen in the 6.9–7.05 region is a blend of two narrow lines (Fe XXVI and Fe Kβ) rather than a broad Fe Kβ line arising from the accretion disk. This fit is shown in Fig. 5.
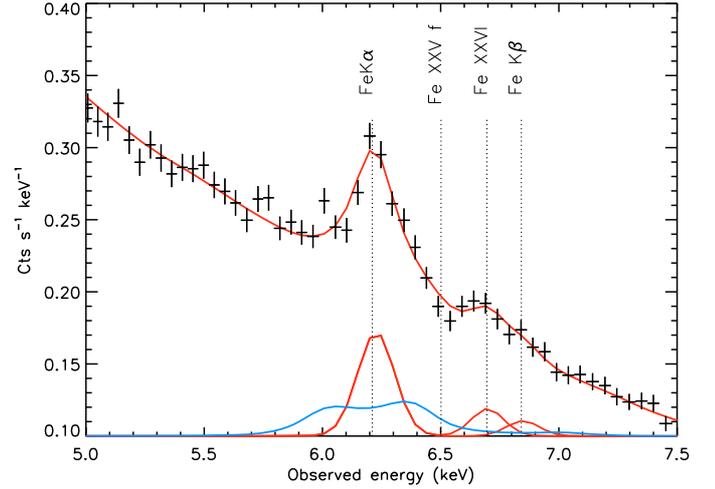
Fig. 5. Spectrum and best fit in the iron line region as observed by Epic-PN. The solid lines display the broad and narrow components added to fit the emission features: a prominent Fe Kα line and weaker lines identified as Fe XXVI and Fe Kβ.

The reduced χ^2 of a fit with all emission lines included, but no absorption, is 308/238. With this final component (see below), the $\chi^2/\nu = 281/234 \sim 1.2$. The lines' parameters and their significance are listed in Table 3. In all the lines fitting, we also let the normalization free to vary towards negative values. This allowed us to use the F-test as an indication of the significance of the lines (Protassov et al. 2002).

2.3. The underlying absorption

Mrk 279 shows a complex absorption spectrum (C07), whose characteristics are best studied using RGS. In analogy with C07, we modeled the absorption with two Galactic components, that is a neutral gas ($N_H = 1.64 \times 10^{20}$, Elvis et al. 1989) and a ionized gas, highlighted by the O VII absorption line at 21.6 Å, with $N_H \sim 3.6 \times 10^{19}$ cm^{-2} and temperature $T \sim 7.2$ eV (C07, Williams et al. 2006). Further, we detect other two, photoionized, gas components intrinsic to the source. We report the average physical parameters of the warm absorbers as measured by RGS and the Epic-PN in Table 5. The absorbers are characterized by a low N_H. Therefore absorption lines, well detected in the high-resolution spectrum (Fig. 3), rather than edges (which are in this case shallow features in the Epic spectrum), are the signature of the absorbers. The inclusion of a lower ionization gas alone already improves the Epic-PN fit by $\Delta\chi^2/\Delta\nu = 17/2$. The inclusion of a two-component gas, with column densities and ionization parameters free to vary leads to an improvement of the fit of $\Delta\chi^2/\Delta\nu = 27/4$, bringing the reduced χ^2/ν to ~ 1.20. A detailed analysis of the complex absorption and a comparison with previous results will be presented in a forthcoming paper (Ebrero et al., in prep.).

3. Modeling of the Fe Kα line region

In this section we evaluate the contribution of different region in the proximity of the AGN to the spectrum above 6 keV.

3.1. The LOC model for the broad emission lines

Here we investigate a possible physical link between the Fe Kα line and the optical BLR. In order to quantitatively evaluate the

Table 5. Best fit parameters for the absorbed spectrum as measured by RGS and Epic-PN.

Comp.	Param.	RGS	PN
1	N_H	0.7 ± 0.2	1.5 ± 0.5
	$\log \xi$	0.8 ± 0.3	1.1 ± 0.3
	v_{out}	-300 ± 150	-300 fix.
2	N_H	3 ± 1	4 ± 1
	$\log \xi$	2.6 ± 0.1	1.8 ± 0.1
	v_{out}	-400 ± 150	-400 fix.

Notes. For each component we list the column densities (N_H) in units of 10^{20} cm^{-2}, ionization parameter ($\log \xi$) and outflow velocities (v_{out}, in km s^{-1}).

Fig. 6. The SED of Mrk 279 in 2005 measured by XMM-*Newton* (solid line). The optical data are measured by OM, while the broad band X-ray continuum is measured by Epic-PN. The dotted line shows the SED of the 2003 data for comparison (C07).

Fig. 7. The solid thick line shows the predicted BLR line luminosities in the X-ray band in units of 10^{40} erg s^{-1} using the LOC model, using as constraints $C_V = 34 \pm 26\%$ and the observed luminosity of the broad O VII line. The value of γ is consistent with what previously found for Mrk 279. The asterisks are the value of the observed broad line luminosities by XMM (Table 3). The dashed line shows the LOC modeling based on the 2003 SED and observed O VII line luminosity. The filled triangle shows the O VII broad line luminosity observed by *Chandra*.

contribution of the BLR to any X-ray broad lines, we used the "locally optimally emitting clouds" model (Baldwin et al. 1995). This model considers the observed line luminosity as a sum of lines emitted at different density n and distances r, weighted by a powerlaw distribution for n and r: $n^{-\beta}$ and $r^{-\gamma}$ respectively (see e.g. C07, Korista et al. 1997, for details). For the present observation we can benefit from the results obtained in C07: they evaluated the "structure" of the BLR (i.e. the distribution of r and the covering factor) fitting 11 UV lines observed by HST-STIS and FUSE simultaneously to the *Chandra*-LETGS data. They found a slope for r, $\gamma = -1.02 \pm 0.14$ and a covering factor $C_V = 34 \pm 26\%$, keeping the slope for n fixed to -1 (Korista & Goad 2000). The general structure of the BLR is not expected to have changed significantly in the 2.5 years that have elapsed since the *Chandra* observation. Therefore we apply those value also to the present spectral energy distribution (SED).

However, the ionizing continuum, and as a consequence the line luminosities, may have changed. In Fig. 6 the SED used for the present observation (2005) is displayed (solid line). The optical points are measured by OM using the U (344 nm), $UVW1$ (291 nm), $UVM2$ (231 nm) and $UVW2$ (212 nm) filters. The unabsorbed X-ray continuum is evaluated using the Epic-PN data. For energies higher than 10 keV, the power law continuum was extended and artificially cut off at $\sim$150 keV. On the very low energy end of the SED (far infrared to radio band), the shape was taken from a standard AGN SED template used in Cloudy (Ferland 2004). We used Cloudy (version 07.02.02, Ferland et al. 1998) to calculate a line luminosity grid over a large range of r and n values. As in C07, r ranged between $10^{14.7-18}$ cm. The value of n ranged between $10^{8-12.5}$ cm^{-3}. For both parameters the spacing of the values was 0.125 in log. For comparison, we show also the SED used for the 2003 observation. The overall optical flux is higher for the present data, while the X-ray continuum remained almost unchanged in flux and soft X-ray spectrum.

In order to infer the BLR contribution to the Fe Kα line, we have to rely on the O VII triplet in the X-ray band, whose luminosity could be totally accounted for by the LOC model (C07). Therefore we assume that all the emission from the broad line of the O VII triplet comes from the BLR. The O VII line luminosity ($L_{OVII} = 13 \pm 7 \times 10^{40}$ erg cm^{-2} s^{-1}) from the RGS data can be explained by the LOC model using the new 2005 SED, with the values of γ and C_V set by the previous analysis, within the errors. Given these constraints, the resulting value for $\gamma = 1.17 \pm 0.03$, which is here the only free parameter, is found to be consistent with previous results. Once this constraint is set, we can predict also the contribution of the Fe Kα and other X-ray lines.

In Sect. 2.2 we have provided two statistically acceptable descriptions of the Fe Kα line: a narrow+very-broad component model and a single, resolved, Gaussian. Only for the latter case

the *FWHM* is similar to the one directly measured from the UV data ($FWHM_{UV} = 8500-9500$ km s^{-1}, Gabel et al. 2005). In Fig. 7 we show the BLR line luminosities predicted by the LOC model in the X-ray band. Along with the O VII observed luminosity we also plot the observed value for the Fe Kα line in the case of a single Gaussian model (Table 3). The predicted O VII/Fe Kα luminosity ratio is about 6.3 within the narrow 1.14−1.20 range for γ. Therefore, the BLR contribution to the Fe Kα line is then $L_{BLR}(\text{Fe K}\alpha) = 2 \pm 1 \times 10^{40}$ erg s^{-1}, about 30 times smaller than the broad Fe Kα component measured from the data. For comparison we also made a prediction on the iron line flux based on the 2003 SED and the BLR parameters derived in C07. In that case the Fe Kα luminosity of iron from the BLR is $10 \pm 5 \times 10^{40}$ erg s^{-1}.

Table 6. Parameters of the Fe Kα at different epochs.

Year	E (keV)	L (10^{40}erg s^{-1})	FWHM (keV)
2002a	6.43 ± 0.03	46 ± 11	0.26 ± 0.12
2002b	6.42 ± 0.04	41 ± 15	<0.20
2005 obs 1	6.42 ± 0.01	56 ± 8	0.19 ± 0.05
2005 obs 2	6.40 ± 0.02	53 ± 8	0.17 ± 0.05
2005 obs 3	6.42 ± 0.03	86 ± 17	0.3 ± 0.1

Notes. We list the energy, intrinsic luminosity and *FWHM* for a single-line fit to the Fe Kα profile for the spectra obtained in 2005 in three separate orbits and for observations collected in 2002 by XMM-*Newton* (2002a) and *Chandra*-HETGS (2002b).

3.2. Variability of the continuum and iron line complex

Lines emitted at a few gravitational radii from the black hole may show significant short term variability. We examined the Fe Kα line parameters in the three time segments of our observation using a simple Gaussian model. We find that the flux, the *FWHM*, centroid energy and the underlying powerlaw slope are nearly the same in response to the central-source variation. In order to further test a variability of the Fe Kα flux we analyzed both an archival XMM-*Newton*-pn data set with a net exposure time of ~26 ks, collected in May 2002 and *Chandra* HETGS data, collected about 10 days later in May 2002 (Scott et al. 2004; Yaqoob & Padmanabhan 2004). In Table 6 we show the comparison of the line parameters of all observations since 2002, for a single-line model.

Prior to 1994, Mrk 279 showed a significant 2–10 keV flux variation, ranging from $1-5 \times 10^{-11}$ erg cm^{-2} s^{-1} (Weaver et al. 2001). The 2002 *Chandra*-HETGS observation, revealed a very low-flux state of the source (~1.2×10^{-11} erg cm^{-2} s^{-1}, Scott et al. 2004), a factor of two lower than what measured by XMM-*Newton*, shortly before. In the last XMM-*Newton* observation the source shows a 2–10 keV flux of ~2.5×10^{-11} erg cm^{-2} s^{-1}. We see that, despite the change in the continuum flux (a factor two), the Fe Kα line parameters did not dramatically change in three years time, within the errors.

In the *Chandra* data the decline of the HETGS effective area and the low signal-to-noise ratio hampered the detection of the Fe XXVI and Fe Kβ lines. On the contrary, in the 2002 XMM-*Newton* spectrum, both lines, although blended, are detected at about 95 and 90% confidence level for Fe XXVI and Fe Kβ, respectively. The line luminosities are the same we obtain in 2005, within the errors.

3.3. The Fe XXVI line at 6.9 keV

There are no detectable changes in the Fe XXVI line in a 3-years time scale. The absence of any of the lines (or a blend of lines) of the Fe XXV triplet is also peculiar (Table 4, Fig. 5). In order to understand the properties of the gas emitting Fe XXVI, we created a grid of column density, logN_H = 22.0–24.5, and ionization parameter, logξ = 3–7, using Cloudy. For lower-column-density, lower-ionization parameter gas, the predicted emission line would be too weak, or absent. For an easy scaling of the luminosity, we initially considered the covering factor (C_V) equal to unity. This is the fraction of light that is occulted by the absorber[3]. A covering factor of one is of course unrealistic, because

---

[3] This is different from the global covering factor, the fraction of emission intercepted by the absorber averaged over all lines of sight, which is has been estimated to be about 0.5 (e.g. Crenshaw et al. 2003).
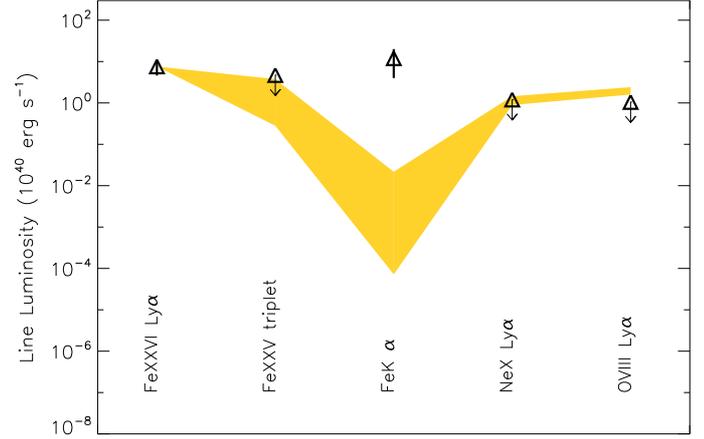
Fig. 8. Emission line contribution to the high ionization lines (Fe XXVI, Fe XXV, Ne X, O VIII). Triangles: data. Light shaded line: range of models viable to fit the data.

in this case absorption lines of the same ions should be observed. Therefore C_V must be less than one. We also simplistically assume that a single gas component is responsible for all Fe XXVI emission. Therefore, we took the measured intrinsic luminosity of Fe XXVI as the reference line to estimate the covering factor. We only have upper limits on other highly ionized lines (namely N VII, O VIII, Ne X and Fe XXV, Table 4), therefore a formal χ^2 fit cannot be performed. However, those limits contain information that can be used to constrain the parameters. In Fig. 8 the set of parameters which are consistent with the measurements are displayed.

In Fig. 9, we show the parameter space of the possible solutions. We see that the ionization parameter sufficient to produce Fe XXVI, but not Fe XXV has to be larger that ~5.3. The ionization parameter linearly correlates with the column density, as for the highest values of logξ the emission lines are visible only if there is sufficient emitting material. For the same reason, for the same column density, logξ and C_V correlate linearly. On the other hand, the covering factor anti-correlates with N_H (Fig. 9). Indeed, for a high column density less material on the line of sight is needed to produce the observed emission.

4. Discussion

4.1. A complex continuum

The continuum spectrum of Mrk 279 needs at least three component to be correctly interpreted: a modified black body and a broken powerlaw (Table 2). In principle, reflection from both the accretion disk and from distant matter should be present (Nandra et al. 2007; Krolik & Kriss 1995; Matt et al. 1991; George & Fabian 1991). The only difference would be that if arising from the accretion disk, the reflection and the associated iron line should be modified by relativistic effects. The harder tail with $\Gamma \sim 1.75$ and the double component of the iron line profile (Sect. 2.2) may be reminiscent of a reflection emission component. We therefore tested this scenario, in comparison with our phenomenological model for the continuum, including both types of reflection in the model (model REFL in SPEX). This model simultaneously considers the Compton reflected continuum (Magdziarz & Zdziarski 1995) and the fluorescent emission from Fe Kα (Zycki & Czerny 1994; Zycki et al. 1999) from a Schwarzschild black hole. General relativity effects and convolution with an accretion disk effects can be easily switched off in this model. Free parameters are the normalization of the
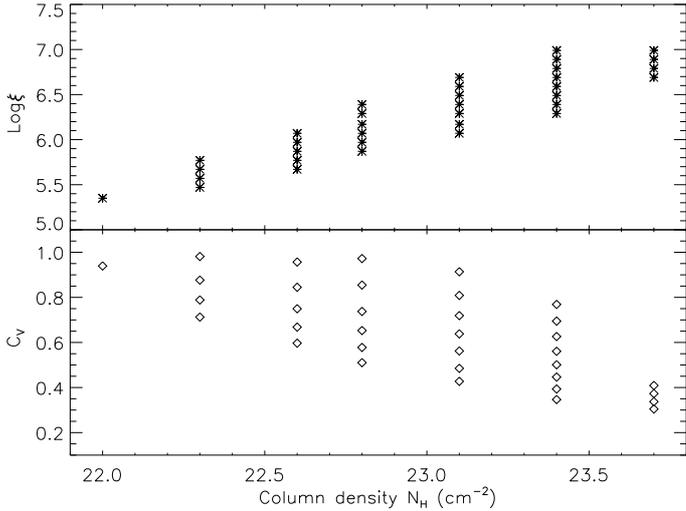
Fig. 9. Parameter space of parameters viable to produce the observed high-ionization emission spectrum. *Upper panel*: Log of the ionization parameter as a function of the log of the column density. *Lower panel*: covering factor of the Fe XXVI line as a function of the log of the column density.

reflected power law and its spectral index Γ, the reflection scale[4] s, the emissivity scale α (Zycki et al. 1999), the inclination angle i of the disk of the iron line emission. In the unblurred reflection, we fixed the inclination angle to 60°, based on the average found for a large sample of Seyferts (Nandra et al. 2007).

We find that the energy range $E > 3$ keV can be well fitted by a combination of a reflector with relativistic properties and by a distant reflector. The former accounts for the broad component of the Fe Kα line, while the latter models the narrow component of the line (Table 7) in a similar way as obtained in the two-component fit (Fig. 5).

The basic parameters of the disk (e.g. the inclination angle, Table 7) are in agreement with what was found from the Fe Kα line fit using the Laor (1991) model. We note however that here a comparison is not straightforward as in Zycki & Czerny (1994) a diskline from a Schwarzschild (rather than Kerr) black hole is included.

The two reflection component cannot fit simultaneously the broad band continuum, as the soft energy portion of the spectrum is significantly underestimated. To reach an acceptable fit, this region has to be modeled again by a modified black body and a single powerlaw (Table 7). Residuals mainly at the crossing points of the continuum components determine the value of the reduced χ^2 (Table 7). Therefore a broad band modeling only in terms of reflection is not straightforward. In addition, hard X-rays coverage is not available and this fit is based on the 0.3–10 keV continuum shape and an iron line with two blended components. This limited knowledge on the broad band behavior makes the fit parameters very uncertain.

4.2. The contribution of the BLR to the Fe Kα line

We have quantitatively evaluated the BLR contribution to the emission of the prominent Fe Kα line at 6.4 keV. The highly ionized specie of Fe XXVI has a negligible role in the BLR, therefore the emission we see at those energies in the X-ray spectrum must

---

[4] The parameter s is a scaling factor for the reflected luminosity: $L_{tot} = L_{pow} + sL_{refl}$. For an isotropic source above the disk $s = 1$, corresponding to an equal contribution from direct and reflected spectrum.

Table 7. Alternative fit of the continuum, including reflection.

T_{mbb}	keV	0.21 ± 0.3
Γ		2.5 ± 0.1
blurred		
$norm_{pow}$	10^{51} ph s^{-1} keV^{-1}	4.1 ± 0.3
Γ		1.73 ± 0.08
α		>1.7
i	deg	<30
s		0.8 ± 0.3
unblurred		
$norm_{pow}$	10^{51} ph s^{-1} keV^{-1}	8.0 ± 2.5
Γ		1.73 ± 0.08
i	deg	60 fixed
s		$1.1^{+1.3}_{-0.2}$
χ^2/ν		322/230

Notes. The model includes a black body, a power law, blurred reflection from the accretion disk and reflection from unblurred cold and distant material. The value of χ^2_{red} refers to full modeling, including absorption (Sect. 2.3) and emission lines (Sect. 2.2).

come from some other location (Sect. 4.4). We based this analysis on previous results for the BLR structure and on the present detection of the O VII broad line in the RGS spectrum. From the extensive experience of broad lines studies in optical spectra of AGN, it is known that measurements of broad and shallow emission features can be affected by large uncertainties and should be cautiously treated. The limitation is due for instance to the signal-to-noise ratio of the continuum level. Resolution, effective area and calibration of the instrument are also relevant effects. However, known, possibly not completely calibrated, instrumental narrow features (23.05, 23.35 Å, de Vries et al. 2003) fall at the border of the O VII emission region. Observation-specific bad pixels (flagged as bad channels in the spectrum) are automatically taken into account when computing the instrument response, but they may certainly cause additional uncertainty when fitting narrow features. The O VII broad line is 1.4 Å wide and the determination of its flux is not significantly influenced by bad pixels. Considering also the very significant, independent, detection in the *Chandra*-LETGS data, we treat this feature as an intrinsically-low-flux O VII line. The line flux measured in 2005 is indeed weaker than in 2003 (Sect. 2.2), even though the SED of 2005 shows an increased availability of optical and UV photons (Fig. 6). Such a behavior of the line intensity is however not unexpected, as the single line luminosities are also sensitive to the long term flux history and the shape of the SED both in the UV and X-ray band (at least of the previous two months, given the typical size of the BLR). The X-ray continuum of Mrk 279 has been observed to change in a month time-scale (Sect. 3.2), however the information on the light curve of Mrk 279 is sparse, as the most recent observation prior to the XMM-*Newton* pointing has been done in 2003 (C07). Therefore a reconstruction of the SED prior to the present XMM-*Newton* observation cannot be performed. In this study we find that only a small fraction of the broad Fe Kα line can be produced in the BLR. From the LOC modeling we find that the Fe Kα line luminosity, coming from the BLR, should be about six times smaller than the O VII triplet. This translates in a contribution to the Fe Kα line which is about 30 times smaller than that observed, implying a 3% contribution. However, the elemental abundance close to a black hole, especially of iron, might be different from Solar. Abundances up to 7 times Solar have been suggested (e.g. Fabian et al. 2002). The same BLR model, but with the Fe abundance enhanced by a factor seven only reduces the O VII/Fe Kα luminosity ratio to about

4.5. However, such an overabundance implies much stronger X-ray iron lines from the L–M shells, which are not observed. If we artificially consider the luminosity of the Fe Kα as entirely produced in the BLR, we should observe an O VII line with a luminosity as large as 3×10^{42} erg s^{-1}, which is clearly inconsistent with both the present and archival measurements (C07). Moreover the Ne IX and O VIII broad lines (with predicted luminosity of about 60×10^{40} erg s^{-1}) would be clearly visible in the spectrum, against the observational evidence. The same discrepancy applies if we consider the very broad profile of the Fe Kα line as arising from the BLR (Sect. 2.2). In that case, the BLR contribution would be 23 times smaller than observed. The unresolved component of the Fe Kα would instead be about 6 times smaller. If this were the case, the contribution of the BLR to the Fe Kα line would not be negligible ($\sim$16%). However, the *FWHM* of the core of the Fe Kα line, as measured by *Chandra*-HETGS is 4200^{+3350}_{-2950} km s^{-1} (Nandra 2006), which is inconsistent with the *FWHM* of the UV lines (Gabel et al. 2005). Moreover, BLR line are subjected to significant variability both in the UV (e.g., Goad & Koratkar 1998) and in the X-rays (Steenbrugge et al. 2009; and present work), while we could not detect any significant change in the iron line flux, measured in a few occasions by different instruments (Sect. 3.2). This also supports the idea that the BLR contribution should be minimal. An important note is that the BLR parameters of Mrk 279 were determined first using UV data only (see C07 and Sect. 3.1) and then applied to the X-ray data. With this approach, any X-ray line only provides useful upper limits, within the range imposed already by the C_V value, on the normalization of the LOC model (Fig. 7). Therefore, in principle, given a BLR model and an SED, the contribution of the BLR to the Fe Kα line can be calculated without the support of other X-ray lines. As a test, we also predicted the iron line luminosity considering the SED and BLR parameters derived for the 2003 data set. In that case, reminding that we do not have any simultaneous measurement of the Fe Kα line in 2003, the contribution of the BLR to the line would be roughly 17%.

Here for the first time we have tested the connection between the optical BLR and the Fe Kα line, using the intrinsic luminosity of the lines (rather than the *FWHM*) and relying on a possible physical model for the BLR (the LOC model, Baldwin et al. 1995). The idea of a non-relation between the BLR and the Fe Kα line has been already tested comparing the width of the optical broad lines with the width of Fe Kα line (e.g. Sulentic et al. 1998; Nandra 2006). In at least one case, (the LINER galaxy NGC 7213, Bianchi et al. 2008) a simultaneous optical-X-ray observation revealed the same width for the Hα and Fe Kα lines, suggesting a common origin in the BLR. However the UV and X-ray lines might come in regions closer to the black hole with respect to the lower ionization lines in the optical, implying a larger *FWHM*. Moreover NGC 7213 can be considered an outsider object, as has been proven to totally lack the reflection component (Bianchi et al. 2003). Therefore a direct comparison with classical Seyfert 1 galaxies (as is Mrk 279) may not be possible.

4.3. The origin of the Fe Kα line

Any variability of the iron line would easily suggest a close interaction between the central source and the region producing the iron line, e.g. the accretion disk. The line does not need to be relativistically smeared, as also Gaussian-shaped lines may arise from the accretion disk (Yaqoob et al. 2003). Using ASCA data Weaver et al. (2001) found variability in the line centroid at

the 1.6σ level (90% confidence). The variability was observed on a time scale of about 20 ks following a 2–10 keV central-flux variation of $\sim$15%. The average EW and *FWHM* as measured by ASCA were however consistent with the present XMM-*Newton* data. Over a time scale of at least 3 years, the Fe Kα line are, in first approximation, stable in luminosity, width and centroid energy within the errors (Table 6). To which extent the line is stable is difficult to assess, as some measurements are affected by large uncertainties. Formally, the line could have changed of as much as a factor of two or more in luminosity. In a scenario where a dominant component of the line does not respond to the central source variation, an origin of the iron line in the accretion disk can be justified by light-bending (e.g. Fabian & Vaughan 2003; Gallo et al. 2007). In that case the apparent flux is allowed to change even of a large factor (up to four) while the line-flux change is marginal (Miniutti et al. 2003). A number of factors may influence the iron line behavior. The limited knowledge of the exact nature of the emission components (both Fe Kα line and continuum) in this source does not allow us to make predictions on the variation of the line in response to the continuum changes on either short or long time scales.

A symmetric line profile, possibly constant over a long time scale, may also suggest a relatively unperturbed environment, like for example the molecular torus, $\sim$1 pc away from the central source. In the framework of the unification model (e.g. Antonucci 1993), the iron line is a natural consequence of the obscuring torus. In type 1 objects, the expected equivalent width would be of the order of 100 eV. However geometrical effects would easily reduce it of a factor of two (Nandra et al. 2007; Krolik & Kallman 1987). In the case of Mrk 279, the EW of the narrow iron line is 70 ± 15 eV, in agreement with the theoretical prediction. The presence of Fe Kβ, insures that the ionization state of iron is less than Fe XVII (Yaqoob et al. 2007). A further constraint on the ionization state of iron would be based on the Fe Kα/Fe Kβ branching ratio, which ranges from 0.12 for Fe I up to 0.17 for Fe IX (Palmeri et al. 2003). Unfortunately, considering the associated errors on the observed line fluxes, we only obtain a lower limit of 0.1 to that ratio.

4.4. The nature of the Fe XXVI line

He-like, sometimes associated with H-like, iron lines have been detected in a number of AGN spectra. These lines can be associated to high column density, photoionized gas (Longinotti et al. 2007; Bianchi et al. 2005, and references therein). The spectrum of Mrk 279 does exhibit a narrow emission line at $\sim$6.9 keV, consistent with emission from Fe XXVI, but interestingly Fe XXV is not detected, showing the presence of extremely highly ionized gas. Interpreting this emission as a product of photoionization, we find that a high column-density ($N_H \sim 10^{23}$ cm^{-2}) with a very-high ionization parameter ($\log \xi \sim 6$) is necessary. A range of N_H and $\log \xi$ and covering factors is allowed to explain the Fe XXVI emission and at the same time be consistent with the measured upper limits on the other high ionization lines: Fe XXV, Ne X and O VIII (see Sect. 3.3 and Fig. 9). The covering factor is on average 0.65. As we do not see any associated absorption, this gas must be out of our line of sight. The EW of the Fe XXVI line (12 ± 5 eV) is consistent with an origin in photoionized circumnuclear gas at the distance of the obscuring torus (Bianchi & Matt 2002). The torus itself would produce the bulk of the neutral-weakly ionized iron emission, while a highly ionized outer layer of photoionized gas would be responsible for H-like and He-like iron. In our case the gas is so ionized to suppress even Fe XXV.

Another possibility is that the Fe XXVI line is formed in a hot galactic wind, driven by starburst activity (Chevalier & Clegg 1985). However, a very hot (log $E \sim 9$–10 keV) plasma would be needed to produce the observed Fe XXVI line luminosity via collisional ionization. Such high temperatures have been proposed for example for the diffuse emission of the Galactic ridge (e.g. Tanaka 2002). However, this interpretation is problematic with respect to the confinement of the plasma within the host galaxy, the source of such heat (e.g. Masai et al. 2002) and the contamination by point-like, hard sources in the diffuse emission spectrum (e.g. in NGC 253, Strickland et al. 2002). Another way to model the high ionization spectrum in terms of a galactic wind, is to invoke quasi-thermal acceleration of electrons which then would produce X-rays with thermal photons. Iron lines would be produced by recombination of background iron ions recapturing electrons, as proposed by Masai et al. (2002) for the Galactic ridge emission.

5. Conclusions

We have performed a detailed modeling of the spectrum of Mrk 279, observed for $\sim$160 ks by XMM-*Newton*. Thanks to the broad band coverage we had the opportunity to study in detail both the low-energy emission lines (observed by RGS) and the iron K complex at around 6.4 keV (observed by Epic).

We have extended the "locally optimally emitting cloud" model, which has been conceived to model the UV broad lines coming from the BLR (Baldwin et al. 1995), first to the soft X-ray band (C07) and, in the present paper, to the Fe Kα line. The BLR can easily account for the O VII broad emission (C07), while it contributes marginally to the luminosity of the broad iron line at 6.4 keV (about 3%, this work). This is the first attempt to evaluate the BLR contribution to the luminosity of the iron line using a global modeling (rather than relying on the line *FWHM* only). Further investigation on high quality data of similar sources are of course necessary to test the robustness of our results.

The bulk of the Fe Kα narrow emission line shows no remarkable variability, in flux and shape over at least three years (Sect. 3.2) and it may be produced by reflection from distant and cold matter. The EW of the line ($\sim$70 eV) is also consistent with this picture.

The very broad component of the Fe Kα line may be modeled by a line arising from an accretion disk, associated with relativistically smeared reflection. However, a formal fit using broad-band reflection models is affected by large uncertainties and degeneracy of the parameters, as we cannot access the region above 10 keV and we only have to rely on the Fe Kα profile, which is in turn formed by two line-components.

We also detected emission from Fe XXVI, but not from Fe XXV. This implies an extremely highly ionized medium. Using the available constraints on other highly ionized ions (e.g. Ne X, O VIII and N VII) we could limit the column density of such gas $10^{22} < N_{\rm H} < 5 \times 10^{23}$ cm^{-2} with an increasingly higher ionization parameter $5.3 < \log \xi < 7$. The covering factor of the gas is 0.65 on average. Such a gas is predicted by the AGN unification model, and it could be associated with a highly ionized outer layer of the obscuring torus (e.g. Krolik & Kallman 1987).

References

Anders, E., & Grevesse, N. 1989, Geochim. Cosmochim. Acta, 53, 197
Antonucci, R. 1993, ARA&A, 31, 473
Antonucci, R. R. J., & Miller, J. S. 1985, ApJ, 297, 621
Baldwin, J., Ferland, G., Korista, K., & Verner, D. 1995, ApJ, 455, L119
Bianchi, S., & Matt, G. 2002, A&A, 387, 76
Bianchi, S., Matt, G., Balestra, I., & Perola, G. C. 2003, A&A, 407, L21
Bianchi, S., Matt, G., Nicastro, F., Porquet, D., & Dubau, J. 2005, MNRAS, 357, 599
Bianchi, S., La Franca, F., Matt, G., et al. 2008, MNRAS, 389, L52
Branduardi-Raymont, G., Sako, M., Kahn, S. M., et al. 2001, A&A, 365, L140
Chevalier, R. A., & Clegg, A. W. 1985, Nature, 317, 44
Costantini, E., Kaastra, J. S., Arav, N., et al. 2007, A&A, 461, 121 (C07)
Crenshaw, D. M., Kraemer, S. B., & George, I. M. 2003, ARA&A, 41, 117
de Vries, C. P., den Herder, J. W., & Kaastra, J. S. 2003, A&A, 404, 959
Elvis, M., Wilkes, B. J., & Lockman, F. J. 1989, AJ, 97, 777
Fabian, A. C., & Vaughan, S. 2003, MNRAS, 340, L28
Fabian, A. C., Ballantyne, D. R., & Merloni, A. 2002, MNRAS, 331, L35
Ferland, G. J. 2004, American Astronomical Society Meeting Abstracts, 205
Ferland, G. J., Korista, K. T., Verner, D. A., et al. 1998, PASP, 110, 761
Gallo, L. C., Brandt, W. N., & Costantini, E. 2007, MNRAS, 377, 391
Gabel, J. R., Arav, N., Kaastra, J. S., et al. 2005, ApJ, 623, 85
George, I. M., & Fabian, A. C. 1991, MNRAS, 249, 352
Ghisellini, G., Haardt, F., & Matt, G. 1994, MNRAS, 267, 743
Goad, M., & Koratkar, A. 1998, ApJ, 495, 718
Jiménez-Bailón, E., Piconcelli, E., & Guainazzi, M. 2005, A&A, 435, 449
Kaastra, J. S., & Barr, P. 1989, A&A, 226, 59
Kaastra, J. S., Steenbrugge, K. C., & Raassen, A. J. J. 2002, A&A, 386, 427
Kaastra, J. S., Raassen, A. J. J., Mewe, R., et al. 2004, A&A, 428, 57
Korista, K., Baldwin, J., Ferland, G., & Verner, D. 1997, ApJS, 108, 401
Korista, K. T., & Goad, M. R. 2000, ApJ, 536, 284
Krolik, J. H., & Kallman, T. R. 1987, ApJ, 320, L5
Krolik, J. H., & Kriss, G. A. 1995, ApJ, 447, 512
Krolik, J. H., Madau, P., & Zycki, P. T. 1994, ApJ, 420, L57
Laor, A., 1991, ApJ 376, 90
Longinotti, A. L., Bianchi, S., & Santos-Lleo, M. 2007, A&A, 470, 73
Masai, K., Dogiel, V. A., Inoue, H., Schönfelder, V., & Strong, A. W. 2002, ApJ, 581, 1071
Magdziarz, P., & Zdziarski, A. A. 1995, MNRAS, 273, 837
Matt, G., Perola, G. C., & Piro, L. 1991, A&A, 247, 25
Miniutti, G., Fabian, A. C., Goyder, R., & Lasenby, A. N. 2003, MNRAS, 344, L22
Nandra, K. 2006, MNRAS, 368, L62
Nandra, K., O'Neill, P. M., George, I. M., & Reeves, J. N. 2007, MNRAS, 382, 194
Ogle, P. M., Mason, K. O., & Page, M. J. 2004, ApJ, 606, 151
Palmeri, P., Mendoza, C., Kallman, T. R., Bautista, M. A., & Meléndez, M. 2003, A&A, 410, 359
Peterson, B. M. 1993, PASP, 105, 247
Pounds, K. A., Reeves, J. N., King, A. R., & Page, K. L. 2004, MNRAS, 350, 10
Protassov, R., van Dyk, D. A., Connors, A., Kashyap, V. L., & Siemiginowska, A. 2002, ApJ, 571, 545
Reynolds, C. S., & Nowak, M. A. 2003, Phys. Rep., 377, 389
Scott, J. E., Kriss, G. A., Lee, J. C., et al. 2004, ApJS, 152, 1
Steenbrugge, K. C., Kaastra, J. S., Crenshaw, D. M., et al. 2005, A&A, 434, 569
Steenbrugge, K. C., Fenovčík, M., Kaastra, J. S., Costantini, E., & Verbunt, F. 2009, A&A, 496, 107
Strickland, D. K., Heckman, T. M., Weaver, K. A., Hoopes, C. G., & Dahlem, M. 2002, ApJ, 568, 689
Sulentic, J. W., Marziani, P., Zwitter, T., Calvani, M., & Dultzin-Hacyan, D. 1998, ApJ, 501, 54
Tanaka, Y. 2002, A&A, 382, 1052
Tanaka, Y., Nandra, K., Fabian, A. C., et al. 1995, Nature, 375, 659
Weaver, K. A., Gelbord, J., & Yaqoob, T. 2001, ApJ, 550, 261
Williams, R. J., Mathur, S., & Nicastro, F. 2006, ApJ, 645, 179
Wilms, J., Reynolds, C. S., Begelman, M. C., et al. 2001, MNRAS, 328, L27
Yaqoob, T., & Padmanabhan, U. 2004, ApJ, 604, 63
Yaqoob, T., George, I. M., & Kallman, T. R. 2003, ApJ, 596, 85
Yaqoob, T., Murphy, K. D., Griffiths, R. E., et al. 2007, PASJ, 59, 283
Young, A. J., Lee, J. C., & Fabian, A. C. 2005, ApJ, 631, 733
Zycki, P. T., & Czerny, B. 1994, MNRAS, 266, 653
Zycki, P. T., Done, C., & Smith, D. A. 1999, MNRAS, 305, 231